The Force Exerted by a Single Kinesin Molecule Against a Viscous Load

Alan J. Hunt,* Frederick Gittes,‡ and Jonathon Howard*
*Department of Physiology and Biophysics, and ‡Center for Bioengineering, University of Washington, Seattle, Washington 98195 USA

ABSTRACT Kinesin is a motor protein that uses the energy derived from the hydrolysis of ATP to power the transport of organelles along microtubules. To probe the mechanism of this chemical-to-mechanical energy transduction reaction, the movement of microtubules across glass surfaces coated with kinesin was perturbed by raising the viscosity of the buffer solution. When the viscosity of the solution used in the low density motility assay was increased approximately 100-fold through addition of polysaccharides and polypeptides, the longer microtubules, which experienced a larger drag force from the fluid, moved more slowly than the shorter ones. The speed of movement of a microtubule depended linearly on the drag force loading the motor. At the lowest kinesin density, where dilution experiments indicated that the movement was caused by a single kinesin molecule, extrapolation of the linear relationship yielded a maximum time-averaged drag force of 4.2 ± 0.5 pN per motor (mean ± experimental SE). The magnitude of the force argues against one type of "ratchet" model in which the motor is hypothesized to rectify the diffusion of the microtubule; at high viscosity, diffusion is too slow to account for the observed speeds. On the other hand, our data are consistent with models in which force is a consequence of strain developed in an elastic element within the motor; these models include a different "ratchet" model (of the type proposed by A. F. Huxley in 1957) as well as "power-stroke" models.

INTRODUCTION

Cellular motility is mediated by motor proteins, such as myosin, dynein, and kinesin, which are enzymes that convert the chemical energy derived from the hydrolysis of the gamma phosphate bond of ATP into mechanical work. Myosin drives muscle contraction by tugging on actin filaments, dynein propels the beating of sperm by shearing contiguous microtubules, and kinesin transports organelles by carrying them along microtubules.

The standard model for chemomechanical transduction postulates a cyclic reaction between the motor and the filament (Huxley, 1969; Lymn and Taylor, 1971). After binding to the filament, the motor is thought to undergo a structural change, the power stroke, that produces an increment of movement. The protein then releases the filament before rebinding to a different site on the filament, thereby initiating another cycle. Support for this model derives mainly from biochemical studies performed in solution, which show that the ATP hydrolysis reaction is a sequential one in which the motor has high affinity for the nucleotide or for the filament, but not for both. The motor must bind to the filament to catalyze product release (for kinesin, see Hackney, 1988) and, after product release, the motor must bind ATP to catalyze filament release (for kinesin, see Brady, 1985; Vale et al., 1985a).

This model has been difficult to test because the molecular events underlying the motor reaction—the distance moved per ATP hydrolyzed, the force generated by a single motor molecule, and the transition rates between the various mechanical and biochemical states—remain obscure. There are two main reasons for this. First, the sheer number of motor molecules in active cells like muscle fibers and sperm has made it difficult to extrapolate the results of mechanical experiments on whole cells down to the single molecule level. Second, the interpretation of biochemical studies of the ATP hydrolysis mechanism is restricted because in solution the motors are unloaded, and, at least in muscle, load also has a dramatic effect on the reaction (Fenn, 1924; Hill, 1938). The development of in vitro motility assays, which permit the study of motility by a small number of purified motor molecules (Sheetz and Spudich, 1983; Allen et al., 1985; Vale et al., 1985b; Kron and Spudich, 1986), promises to circumvent these two problems.

We have chosen kinesin as a model motor for study because single molecules of kinesin are sufficient to generate motility in vitro (Howard et al., 1989; Block et al., 1990). Studying single motors is important because even in vitro, motors acting on the same filament can interact (for myosin, see Warshaw et al., 1990) and thereby obscure the underlying events. Unlike myosin and flagellar dynein, which operate in large arrays in vivo, kinesin operates alone or in small numbers to move vesicles along microtubules (Miller and Lasek, 1985). This property of kinesin has permitted the development of assays in which the motility of a single kinesin molecule can be studied: microtubules glide across glass surfaces that are very sparsely coated with kinesin, and the diffusive rotatory motion superimposed on the microtubule's directed translation indicates that the microtubule is attached to the surface at only a single point, the location of the motor (Howard et al., 1989; Hunt and Howard, 1993a). Dilution experiments indicate that the functional motor is a single kinesin molecule (Howard et al., 1989; Block et al., 1990).

Several mechanical properties of kinesin have been deduced from in vitro motility assays. Kinesin moves toward

Received for publication 3 February 1994 and in final form 13 May 1994.
Address reprint requests to Jonathon Howard, Department of Physiology and Biophysics, SJ-40, Room G424, Health Sciences Building, University of Washington, Seattle, WA 98195. Tel.: 206-685-3199; Fax: 206-685-0619; E-mail: jhoward@u.washington.edu.

0006-3495/94/08/766/16 $2.00

the plus, or fast-growing, end of the polar microtubule filament (Vale et al., 1985a; Howard and Hyman, 1993). The high torsional flexibility of kinesin allows kinesin, when fixed to a glass surface, to move microtubules equally quickly in any direction with the minus end always leading (Hunt and Howard, 1993a). Microtubules are typically composed of 13 parallel protofilaments in which the 8 nm long tubulin dimers are arranged head-to-tail (Amos and Klug, 1974). Observations of the rotation of microtubules of various protofilament number indicate that kinesin follows a path parallel to the protofilaments with high fidelity (Ray et al., 1993). Because there appears to be only one high affinity kinesin binding site per dimer (Harrison et al., 1993; although steric interference of neighboring kinesin molecules has not been ruled out), kinesin's *step size*, defined as the distance between sites on the microtubule surface to which kinesin consecutively binds, must be a multiple of 8 nm, the interdimer distance. High sensitivity displacement measurements show that under some circumstances kinesin dwells at 8-nm intervals as it moves along the microtubule (Svoboda et al., 1993), indicating that the step size is probably 8 nm. This step size is consistent with the speed with which single kinesin molecules can move microtubules (500–1000 $nm \cdot s^{-1}$) because, in solution, each of kinesin's two motor domains can hydrolyze ATP at a rate as high as 50–100 s^{-1} (cycle times of 10–20 ms) (Kuznetsov et al. (1989); but see, e.g., Gilbert and Johnson (1993), who measured a lower ATPase of 10 s^{-1}).

The pressing question is: How does the motor reach the next binding site, a distance of 8 nm away in the direction of the plus end? Because this distance is smaller (only just!) than the length of kinesin's motor domain, ~10 nm (Hirokawa et al., 1989; Scholey et al., 1989), it is conceivable that the step is bridged by a large structural change within the motor. Such a motion has been postulated for myosin (the rotating cross-bridge model; Huxley, 1969) and is compatible with the molecular structure of the myosin motor domain, which has a long α-helical segment that could act like a lever to amplify the displacement associated with the opening and closing of the ATP-binding cleft (Rayment et al., 1993). Alternatively, instead of one large motion, the distance could be spanned by a diffusive process that is somehow directed by the motor's ATP-hydrolysis mechanism (Huxley, 1957; Braxton, 1988; Braxton and Yount, 1989; Vale and Oosawa, 1990; Pate and Cooke, 1991; Cordova et al., 1992).

To answer this question, we have examined how externally imposed forces influence the motion. In this study, the load on a single kinesin molecule has been increased by raising the viscosity of the solution through which the microtubule is moved, and the effect on microtubule gliding speed was measured (Fig. 1). Because the cell's cytoplasm is crowded with cytoskeletal filaments, the mobility of organelles is very low (Luby-Phelps et al., 1986), and so we might expect that an organelle motor like kinesin is well adapted for working against drag forces. Drag forces, in addition to being physiologically relevant, offer the unique advantage that they are present only while the motor is moving: thus, changing the viscosity permits us, with some selectivity, to perturb only the force-generating phase of the motor reaction without influencing any stationary, or non-force-generating phase. Another advantage of this approach is that by increasing the viscosity, diffusion is slowed down, and we can therefore test models in which diffusive motions play a major role. A preliminary report on this work has appeared (Hunt and Howard, 1993b).

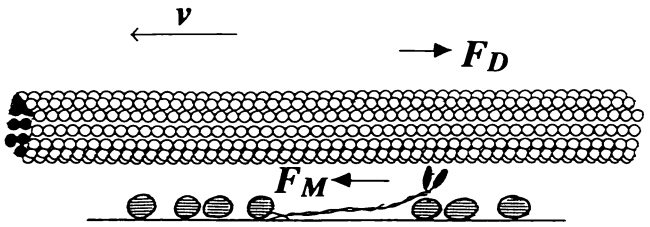

FIGURE 1 A single kinesin molecule attached to a casein-coated (globular objects) glass surface exerts force against a microtubule. The thick arrows indicate the direction of the motor force (F_M) and the viscous drag force (F_D). The thin arrow indicates the direction of microtubule movement at speed v.

MATERIALS AND METHODS

Motility assays

All observations were made in 75-μm-deep perfusion chambers bounded at the bottom by a glass microscope slide and on top by a coverglass (Howard et al., 1989; Howard et al., 1993). The standard buffer solution contained 80 mM Pipes, 1 mM EGTA, and 2 mM $MgCl_2$ and was adjusted to pH 6.9 with KOH. All reagents were obtained from Sigma Chemical Co. (St. Louis, MO). The glass surfaces were precoated by introducing 2.5 mg/ml casein in standard buffer solution into the chamber. Bovine brain kinesin, an $\alpha_2\beta_2$ tetramer (Howard et al., 1993; Hunt and Howard, 1993a), was diluted into standard buffer solution augmented with 250 μg/ml casein, and then introduced at 7–70 ng/ml for nucleotide-free assays, and at 55–100,000 ng/ml for motility assays. The density of kinesin was calculated assuming complete adsorption of kinesin to the glass surfaces during the 5 min allowed for adsorption. This overestimates, by at least a factor of 10, the density of functional kinesin on the coverglass surface at which all of the fluorescence microscopic observations were made; approximately 10-fold higher kinesin concentrations were required to achieve the same rate of microtubule binding to motors on the coverglass surface as on the microscope slide surface (Howard et al., 1993; Hunt and Howard, 1993a).

Both fluorescently labeled (Hyman et al., 1991) and -unlabeled microtubules were polymerized from phosphocellulose-purified bovine brain tubulin (Howard et al., 1989; Howard et al., 1993) and diluted 100- to 1000-fold to ~0.1 mg/ml in standard buffer solution or visc-mix solution (see below) augmented with 10 μM taxol (Drug Synthesis and Chemistry Branch, National Cancer Institute, Bethesda, MD) to prevent depolymerization. In some cases, the microtubules were triturated to lengths of 1–5 μm by passing the solution through a 30-gauge needle before introduction into the perfusion chamber. After introduction of the microtubules, the ends of the perfusion chambers were sealed with grease to prevent fluid flow caused by evaporation.

Temperature was regulated to between 28 and 33°C using either a temperature-regulated blow dryer to heat the general vicinity of the perfusion chamber and microscope or by circulation of heated water through a copper coil wrapped around the microscope objective. The temperature of some perfusion chambers was measured using 50-μm-diameter T-type thermocouple wire (Physitemp Instruments Inc., Clifton, NJ). We estimated that illumination by the 100-W mercury arc lamp raised the temperature in the observation field by less than 1°C.

Digitization of bead and microtubule coordinates

Images were acquired with a silicon-intensified-target camera (Hamamatsu C2400–8, Bartels and Stout, Bellevue) and recorded with a 1/2-inch video cassette recorder (Panasonic AG-7350, Proline, Seattle, WA). Video prints of taped images were made using a Sony UP 5000 video printer. The positions of beads and microtubules were digitized using MEASURE hardware (M. Walsh Electronics, San Dimas, CA) and software generously provided by Dr. S. Block (Rowland Institute, Cambridge, MA; described in Sheetz et al., 1986). Some digitized images were corrected for field distortions in the camera. Typically, the bead and microtubule coordinates were digitized every 3–30 frames (100–1000 ms).

Measurement of microtubule speed

At low viscosity and low kinesin density, the microtubules pivot about the point at which the kinesin molecule is located (Howard et al., 1989). To determine the speed, the distance between the leading end of the microtubule and the fixed point around which it swiveled was measured. The speed (and associated SE) was computed by linear regression from the plot of these distances versus time.

In all other cases, the speed was measured over times when the trajectory of the microtubule was linear: that is, the microtubule did not swivel. A line was fit through the trajectory (in the x-y plane) of the leading end of the microtubule. The distance moved along the trajectory was calculated from the projection of the x-y position onto this linear trajectory. The mean and SE of the speed was then computed from the plot of distance versus time.

Searching for an appropriate viscous solution

When searching for a viscous solution to impose a hydrodynamic drag on the moving microtubules, we ran into two problems: either the solution was hydrodynamically non-ideal (as described below) or it interfered with the motility assays. Solutions of methyl cellulose (Sigma M-0512, 0.3–0.8%, $\eta = \sim 20$–120 mN·s·m^{-2} at a shear rate $s = 45$ s^{-1}; Uyeda et al., 1990; percentages are weight per volume) or high-molecular-weight dextran (Sigma D-5501, molecular weight = 5–40 MDa, 4%, $\eta = 216$ mN·s·m^{-2} at $s = 46$ s^{-1}) suffered from the former problem; the amplitude of the Brownian motion of actin filaments or microtubules in these solutions is much greater in the longitudinal direction, parallel to the filaments' long axes, than in the lateral or perpendicular direction. For a microtubule in a Newtonian fluid, the coefficient of longitudinal diffusion is just under twice that of lateral diffusion in unbounded fluid, and approaches a ratio of two exactly as the microtubule approaches a plane surface (see Appendix A). The quite different behavior of microtubules in the high molecular weight dextran solution is consistent with the idea that the highly elongated solute polymers form a gel whose pore size is greater than the diameter of the cylindrical microtubule; although diffusion parallel to the microtubule's axis through the pores is still possible, diffusion in the perpendicular direction is almost completely suppressed. Such gel-like solutions are not suitable for viscous force measurements.

In light of the above results, it was essential to find a globular, rather than elongated, polymer whose size was less than the diameter of the microtubule. The problem with such agents is that because of their more spherical shape, very highly concentrated solutions are required to increase the viscosity significantly (Van Hold, 1985). We tried many viscous agents; all of them either inhibited motility or bundled microtubules, often at relatively low viscosity. These effects are likely to be chemical in origin, rather than viscous, because different agents produced quite different effects: for example, BSA (20% w/v) caused microtubule bundling, whereas Ficoll-400 (24% w/v) inhibited motility. Such effects are not surprising when one considers the high concentrations that are necessary to increase the viscosity to 100 times that of water.

The realization that the inhibition was likely to be chemical permitted a solution to the impasse. The trick was to construct a composite liquid, which we called visc-mix, made of a combination of viscous agents such that the concentration of each was insufficient to block motility. This combination of solutes produces sufficiently high viscosities without completely inhibiting the motility.

Preparation of visc-mix

Visc-mix consists of 14.5% w/v trypsin inhibitor (Type II-S: Soybean), 15% dextran (average molecule mass 67 kDa), and 7.5% Ficoll-400 (molecule mass 400 kDa) in standard buffer solution. Before being added to visc-mix, the trypsin inhibitor was dialyzed 4 times for at least 6 h each; otherwise, it would depolymerize microtubules: the first three dialyses were against the standard buffer supplemented with 20% Ficoll-400, and the final one was against standard buffer supplemented with 30% Ficoll-400 to increase the protein concentration, which was monitored by absorbance at 280 nm ($A_{280} = 0.92$ cm^{-1}·(mg/ml)$^{-1}$). Visc-mix was diluted with standard buffer to obtain the desired percent visc-mix concentration.

Macroscopic viscosity of the visc-mix solution

The viscosity of several different concentrations of visc-mix was measured with a cone-plate viscometer (Brookfield model DV-I+, spindle CP-40 or CP-51) as a function of the shear rate, s (Fig. 2 *A*). The solution is non-Newtonian: it is least viscous at the highest shear rates, and the viscosity increases as the shear rate is reduced. The apparent divergence of the viscosity at very low shear rates is explained by the existence of a small but nonzero yield stress σ_0 (Fig. 2 *C*); at this stress value, there is no flow, meaning that the viscosity is infinite for $s = 0$: unstressed visc-mix is a solid.

A finite yield stress is known to occur in, for example, concentrated suspensions. There exist a number of empirical forms for this behavior (Skelland, 1967); these, however, do not agree with our data. Instead, our data are fit very well by the following relation between the viscosity (η) and the shear stress ($\sigma = \eta s$),

$$\sigma/\sigma_0 = 1 + \alpha\, \eta_0/(\eta - \eta_0), \qquad \sigma > \sigma_0;$$

$$\eta = \infty, \qquad s = 0, \qquad \sigma \le \sigma_0.$$

α, η_0, and σ_0 are constants. These equations predict a linear relation between $\sigma = \eta s$ and $1/(\eta - \eta_0)$, with an intercept at $\sigma = \sigma_0$, the yield stress. Such behavior is apparent in Fig. 2 *C*, where $\sigma = \eta s$ is plotted against $1/(\eta - \eta_0)$ for a range of concentrations of visc-mix. The ηs-intercept of each line represents an apparent yield stress on the order of 1 Pa or less—a very small value—which increases with concentration. Separate values of η_0 were chosen for linearity at each concentration, which does not affect the ηs-intercept.

Our viscosity data can also be fit somewhat less well by a divergent power law

$$\eta = \eta_0 \cdot [1 + (s_0/s)^{0.75}].$$

This model, not shown in Fig. 2 *C*, would give non-straight curves running reasonably close to the data points, but curving sharply down to the origin to the left of the data. Power-law behavior with a similar exponent occurs in some entangled polymer solutions; in these cases, one should see the power law break down for small enough s, and the viscosity approach a finite value at $s = 0$, which we do not observe. Nevertheless, the power law is consistent with the data over our range of measurement, and for analytical convenience we use it in our calculation of the non-Newtonian drag force (see Appendix B).

Interestingly, the deviation of visc-mix from Newtonian behavior is primarily a property of the mixture, rather than the components. Individually, the Ficoll-400 and dextran-67 solutions are Newtonian over the range of shear rates examined. But the combination of the two displays most of the non-Newtonian behavior of visc-mix: the solute molecules must interact. The trypsin inhibitor is also somewhat non-Newtonian.

Measuring the concentration of visc-mix solutions

The stickiness of the viscous solutions made them difficult to handle even when positive displacement pipettes were used. The main problem was that the viscosity, the most important property in this study, depended critically on the concentration (Fig. 2, *A* and *B*); thus, small pipetting errors occurring

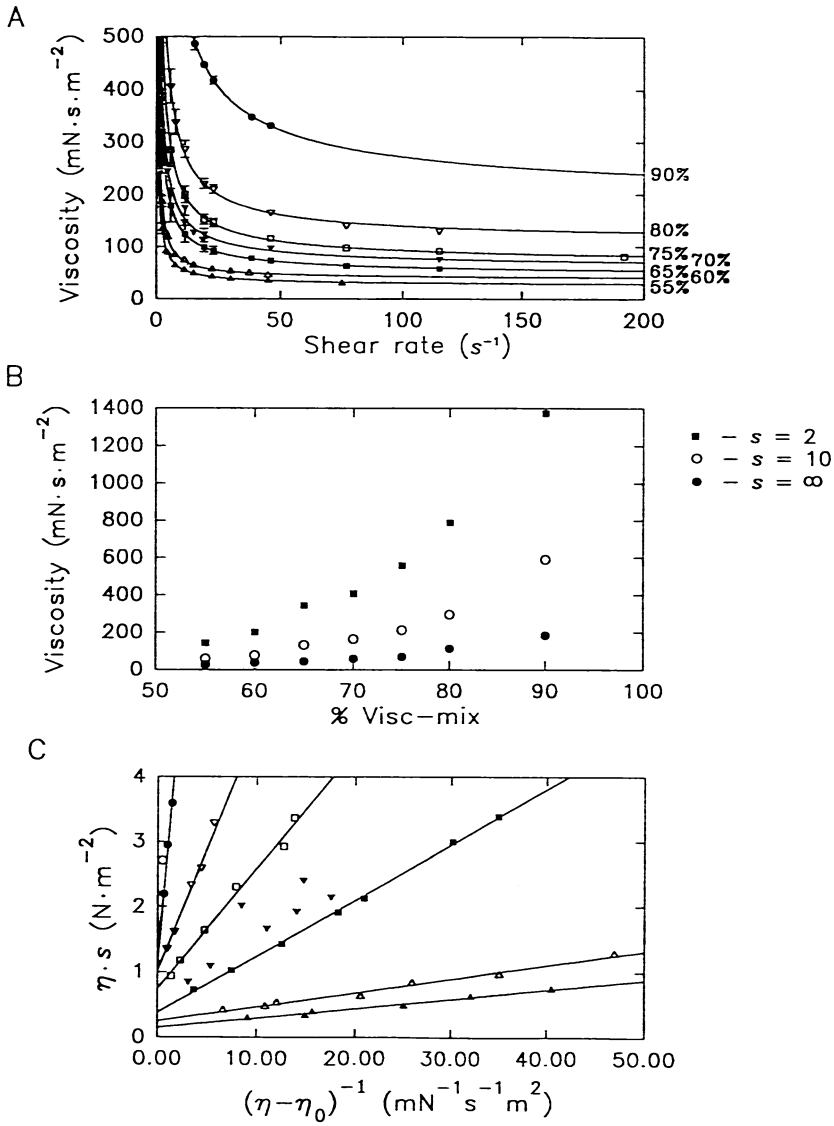

FIGURE 2 (*A*) The viscosity of visc-mix versus the shear rate. The concentration of the visc-mix solution for each curve is indicated on the right. (*B*) Data taken from *A* are replotted to show the relation between viscosity and concentration for visc-mix at three different shear rates. (*C*) The shear stress ηs (note $Nm^{-2} = Pa$) versus the quantity $(\eta - \eta_0)^{-1}$, near the origin, for the same data as in *A*. The ηs-intercept of each line represents an apparent yield stress, which increases with concentration. Separate values of η_0 were chosen for linearity at each concentration, which does not affect the ηs-intercept.

during dilution could cause large changes in the viscosity. Therefore, we used careful measurements of the dependence of viscosity on the concentration of the visc-mix solution (Fig. 2, *A* and *B*) to construct a calibration curve that was used to determine the concentration of a final visc-mix solution from its viscosity.

The steep dependence of viscosity on concentration could lead to a similar problem in the motility experiments; if mixing in the perfusion chambers is incomplete, then we would overestimate the viscosity of the solution through which kinesin moves the microtubules. To minimize this problem, we always perfused with more than 2 times the volume of the perfusion chamber (volume $\approx$ 6.75 μl). To determine the amount of mixing that occurred during this perfusion, a solution containing fluorescent beads was introduced into a perfusion chamber before it was perfused with 80% visc-mix. By comparing the number of beads in the chamber before and after the addition of visc-mix, we estimated that the visc-mix solution was diluted by <1.5% during perfusion into the flow cell, so that the decrease in viscosity was <5%.

Microscopic viscosity of visc-mix

The diameters of trypsin inhibitor and Ficoll-400 are 3.5 and 16 nm, respectively (Sweet et al., 1974; Hou et al., 1990). Assuming that the diameter of dextran varies with the cube root of the molecular weight, we estimate the diameter of dextran-67 to be 6.4 nm from the 4.3 nm hydrodynamic diameter of 20-kDa dextran (Luby-Phelps et al., 1986). Because the sizes of these solute molecules are not that much smaller than the ~30-nm diameter of the microtubules (Beese et al., 1987), we did not know whether the macroscopic viscosity, measured with the cone-and-plate viscometer, applied to the microtubules. In particular, it was essential to confirm that the visc-mix was not behaving as a porous gel like the methyl-cellulose and high molecular weight dextran solutions. As described below, we measured the "microscopic"viscosity of visc-mix by analyzing the Brownian motion of beads and microtubules in it; the Brownian motion was in good agreement with the macroscopic viscosity, and no indications of gel-like behavior were observed.

The microscopic viscosity of the visc-mix solution was measured in several ways. First, the lateral diffusion coefficients of 280 nm diameter fluorescent latex microspheres (Mol. Probes. L-5242) were measured far from the surfaces of the perfusion chamber (>13 μm). The diameters were checked by electron microscopy and by measuring the lateral diffusion coefficient in a glycerol solution of known viscosity (Table 1). Because glycerol solutions are Newtonian and glycerol molecules are very small, the viscosity of glycerol solutions should be well defined both macroscopically and at the microscopic dimensions of microtubules and small beads. The diffusion coefficients D were measured using

$$D = \langle \Delta r^2 \rangle / 4\Delta t = \langle \Delta x^2 + \Delta y^2 \rangle / 4\Delta t, \quad (1)$$

TABLE 1 Microscopic viscosities of visc-mix and glycerol solutions

Particle	Diameter (nm)	Solution	Viscosity* (mN·s·m^{-1})	$D_{measured}/D_{predicted}$	Stokes diameter (nm)
Bead	280	Glycerol	83	0.96 ± 0.07	292 ± 20
Bead	280	78% Visc-mix	75	0.90 ± 0.05	309 ± 17
MT (cm)‡	30	60% Glycerol	13	0.95 ± 0.04	
MT (cm)	30	76% Visc-mix	71	0.64 ± 0.03	
MT (*r*)§	30	60% Glycerol	13	0.79 ± 0.13	
MT (*r*)	30	76% Visc-mix	71	0.64 ± 0.11	
MT (tether)†	30	Water	0.851	=1 by definition	
MT (tether)	30	45% Visc-mix	12.6	0.93 ± 0.20	

* Viscosity at high shear limit (η_0).
‡ Center of mass.
§ Rotatory.
† Rotatory in the tether assay.

where $(\Delta x, \Delta y)$ is the movement in the plane of focus over a time Δt. Equation 1 was averaged over all successive Δt-intervals in a data set, and this was repeated using different values of Δt ($\Delta t = mt_s$, m = 1, 2, 4, 8, 16, and 32 with t_s the sampling interval). The diffusion coefficient calculated in this way was independent of Δt, consistent with the motion being diffusive rather than steady (produced, for example, by fluid flow). The measurement error was negligible; no additional variance attributable to error in measuring the position of the sphere was seen even at the shortest times. The weighted average diffusion coefficient was computed and compared with the theoretical diffusion coefficient for a sphere of radius r predicted by Stokes' Law:

$$D_{sphere} = kT/6\pi\eta r,$$

where k is the Boltzmann constant and T is the absolute temperature.

The diffusion coefficients of the 280-nm beads in visc-mix were consistent with the macroscopic viscosity of visc-mix. In 78% visc-mix, the ratio of the measured diffusion coefficient and the diffusion coefficient predicted from η_0, the high shear viscosity, was 0.90 ± 0.05 (Table 1). Because the average speed of a diffusing bead is very large, the fluid shear around the bead will also be large, and so we expect the high shear viscosity η_0 to be the appropriate measure. This was indeed the case.

Similar experiments were performed using microtubules. In this case, the rotational (D_r) and center of mass (D_{cm}) diffusion coefficients were compared with the theoretical values given by the Einstein relation

$$D = kT/\Gamma,$$

where Γ was predicted from η_0 (Appendix A). The diffusion coefficients were determined from the digitized coordinates of the ends of microtubules projected onto the plane of focus. These microtubules were diffusing approximately 15 μm from the glass surface and were of length $L < 5$ μm. D_{cm} was calculated using Eq. 1, where Δx and Δy are the change in the displacement of the projection of the center of mass of a microtubule calculated as the midpoint between the digitized coordinates of the ends. D_r was calculated using $D_r = \langle\Delta\alpha^2\rangle/4\Delta t$, where $\langle\Delta\alpha^2\rangle$ is the mean-squared change in the microtubule's three-dimensional angle $\Delta\alpha$ measured over time Δt. For each Δt, $\Delta\alpha$ was calculated from digitized coordinates of the microtubule ends according to

$$\Delta\alpha^2 \cong \Delta\theta^2 + \Delta\phi^2 \sin^2\langle\theta\rangle$$

(correct to second order in the angles), where $\Delta\phi$ is the change in the angle of the microtubule projected on the x-y plane (the plane of focus) and $\Delta\theta$ is the change in its angle θ with the z axis. $\langle\theta\rangle$ is the average of θ over Δt. θ was calculated as $\theta = \arcsin(L_{proj}/L)$, where L_{proj} is the projected length of the microtubule onto the x-y plane and L is its actual length, measured as the largest observed value of L_{proj}. All microtubules were observed for at least 2 min. Observations were restricted to values of θ such that there was a less than 5% chance (as predicted from the theoretical diffusion coefficient) of ambiguity caused by crossing $\theta = 0°$ or 90°. As a check of this methodology for measuring microtubule diffusion coefficients, microtubule diffusion was also measured in a glycerol solution (Table 1).

As seen in Table 1, the ratio of the measured diffusion coefficients in visc-mix to those predicted by theory (using η_0 for the viscosity) was 0.64 ± 0.03 for a microtubule's center of mass and 0.64 ± 0.11 for microtubule rotation. The similarity of these values indicates that visc-mix slows diffusion equally in the directions perpendicular and parallel to a microtubule's axis; visc-mix does not display gel-like behavior. We do not understand why these ratios were less than one, as was also found for rotatory diffusion of microtubules in 60% glycerol. A possible explanation for the low ratios is that the small intrinsic curvature of our microtubules (Gittes et al., 1993) gave rise to larger effective hydrodynamic diameters.

Measurement of the viscous drag coefficients for a microtubule tethered to a surface by kinesin: calibration of the viscous force

The parallel drag coefficient, $C_\parallel$, necessary for the calculation of the drag force (Eq. 2), was estimated by first measuring the perpendicular drag coefficient $C_\perp$ in visc-mix, and then using the relation $C_\parallel = C_\perp/2$. This relation, which is discussed in Appendix A for cylinders close to a plane surface, does not hold for solutions containing highly elongated polymers such as methyl cellulose; but as described above, no such gel-like behavior was observed for visc-mix, and so the relation should be valid for our analysis.

$C_\perp$ was estimated by measuring the rotatory diffusion of microtubules tethered to the casein-coated surface by single kinesin molecules (Fig. 3 *A*, Hunt and Howard, 1993a). The rotatory diffusion coefficient was measured by $D_r = \langle\Delta\phi^2\rangle/2\Delta t$, where $\langle\Delta\phi^2\rangle$ is the mean-squared angle fluctuation over time intervals Δt. From the slope of the relationship between the reciprocal

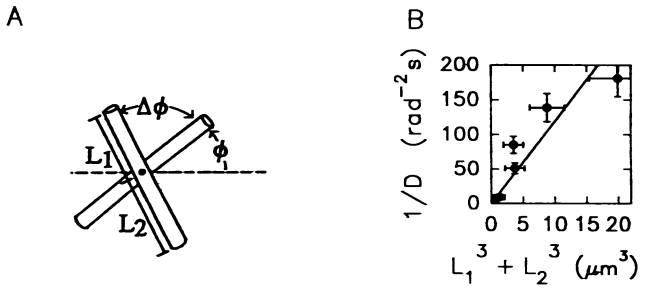

FIGURE 3 (*A*) Drawing of the positions, at two times, of a microtubule tethered to the surface by a single kinesin molecule and undergoing diffusion. Lengths and angles used in the text are defined. (*B*) The rotational diffusion coefficient in 45% visc-mix (η_0 = 12.6 mN·s·m^{-2}) is inversely proportional to the sum of the third powers of the microtubule lengths, $L_1^3 + L_2^3$, defined in *A*.

of D_r and the cube of the microtubule length (Fig. 3 *B*), we deduced $C_\perp$ via

$$\frac{kT}{D_r} = \frac{1}{3} C_\perp \eta (L_1^3 + L_2^3)$$

(Appendix A) where L_1 and L_2 are the microtubule lengths defined in Fig. 3 *A*. In standard buffer solution (η = 0.851 mN·s·m^{-2}), $C_\perp$ was 11.0 ± 1.2 in the absence of ATP and 14.0 ± 1.3 in its presence. These values correspond to nominal distances of 25.7 ± 2.6 and 21.5 ± 1.3 nm from the glass to a microtubule's axis, or 10.7 ± 2.6 and 6.5 ± 1.3 nm from the glass to a microtubule's surface (Hunt and Howard, 1993a). These distances are only approximate because the glass and microtubule do not have the ideal smooth surfaces assumed for the model solved in Appendix A. In practice, the surfaces are bumpy: the advantage of this calibration procedure is that we obtain a direct measure of the drag coefficient without having to assume either the distance between the microtubule and the glass surfaces or the details of the textures of the surfaces. In 45% visc-mix (η_0 = 12.6 mN·s·m^{-2}) and in the absence of ATP, $C_\perp$ was 11.8 ± 2.2, not significantly different from that measured in standard buffer. This is consistent with the suppositions that the distance between the microtubule's axis and the surface is not changed by visc-mix, and that the microscopic viscosity of visc-mix is well predicted by its macroscopic viscosity. Because $C_\perp$ = 14.0 ± 1.3 when measured in the presence of ATP, we used $C_\parallel$ = 7.0 ± 0.7 in Eq. 2 for estimating the drag force through the viscous medium.

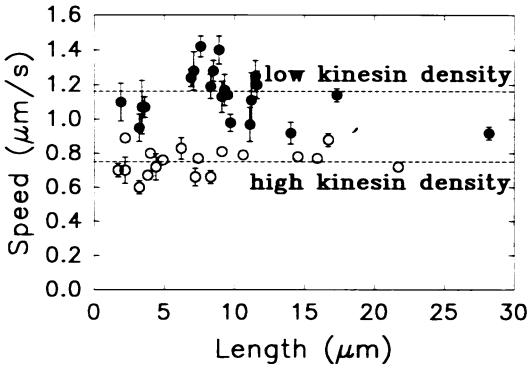

FIGURE 4 In standard buffer (η = 0.8 mN·s·m^{-2}) the speed at which kinesin translates microtubules is independent of the microtubule length. In this figure and Fig. 6 *A*, high kinesin density corresponds to a surface density of ~6000 kinesin molecules/μm^2. Low kinesin density corresponds to 17 kinesin molecules/μm^2 for microtubules ranging from ~0 to 10 μm in length, and 3.4 molecules/μm^2 for microtubules longer than ~10 μm. These surface densities assume complete adsorption of kinesin from the solutions. Not all of the kinesin might be functional.

RESULTS

Kinesin-driven movement through high viscosity solutions

To determine how load influences the kinesin motor, we observed microtubules moving across kinesin-coated glass surfaces through buffer solutions of various viscosities (Fig. 1). The underlying idea is that as the viscosity is increased, the drag force exerted on the microtubule by the solution will approach the maximum force that the motor protein can exert, and so the speed of movement will decrease. The higher the viscosity and/or the longer the microtubule, the greater the drag force and, thus, the smaller the speed of movement. In this way, the relationship between the speed of movement and the drag force can be measured and, by extrapolating to infinite viscosity or infinite microtubule length, the maximum motor force can be estimated.

Low viscosity solutions (η < 1.0 mN·s·m^{-2}) impose virtually no load on kinesin because the longer microtubules move at the same speed as the shorter ones (Fig. 4). This is true regardless of whether the surface is coated with kinesin at high density, in which case we expect that the motion is caused by several kinesin molecules or, at low density, in which case, based on several lines of evidence, the movement is likely caused by single kinesin molecules (see Introduction). For the longest microtubule moving in the low density assay, the time-averaged drag force is 0.18 pN (Eq. 2); because this microtubule is but little slowed compared with shorter ones, it follows that the single motor force must be much greater than 0.2 pN, and that the viscosity of the solution must be raised at least 10- to 100-fold to significantly load a single kinesin motor.

Therefore, we sought and found a high viscosity solution with which we could increase the viscosity of the solution up to 100-fold without poisoning the motor. The solution, which we called visc-mix, was composed of the polysaccharides Ficoll and dextran, and the protein trypsin inhibitor, dissolved in standard buffer solution. When the high density assay was repeated in the presence of 77% visc-mix, sufficient to increase the viscosity about 100-fold (η_0 = 73 mN·s·m^{-2}), microtubules moved smoothly (Fig. 5 *A*) as they did in low-viscosity buffers, and at speeds that were only somewhat less than the speeds in standard buffer (0.50 μm·s^{-1} in visc-mix (Fig. 6 *A*) compared with 0.75 μm·s^{-1} in standard buffer (Fig. 4)). This shows that the motor reaction was not inhibited by these solutes. At high kinesin density and high viscosity, the speed of movement was independent of microtubule length (Fig. 6 *A*). This is not surprising because we expect that the number of motors acting on a microtubule and the viscous drag force should both increase in proportion to a microtubule's length; thus, the longer microtubules will have more motors to overcome the larger drag force.

When the density of kinesin was reduced, microtubule gliding was still observed in high viscosity medium (Fig. 5, *B* and *C*). At the lowest densities, where we expect that the motility is driven by single kinesin molecules, microtubules moved continuously through visc-mix for a number of microns before stopping (2.0 ± 1.0 μm, mean ± SD, n = 6). This behavior is similar to that seen in low viscosity solutions (distance traveled of 3.6 ± 2.7 μm, n = 6). The effect of the high viscosity medium was to reduce the speed of movement of microtubules (Fig. 5, *B* and *C*), consistent with the possibility that the drag force was significantly loading the motors. This interpretation was strengthened by the finding that at kinesin densities less than 10 μm^{-2}, at which we expect that the movement is caused by single kinesin molecules, the longer microtubules moved more slowly than the shorter ones (Fig. 6 *B*). Provided that the microtubules are indeed being moved by single kinesin molecules, and that the slowing is caused by a viscous rather than chemical effect, we can use the speed and length to calculate the drag force and thereby estimate the single-motor force.

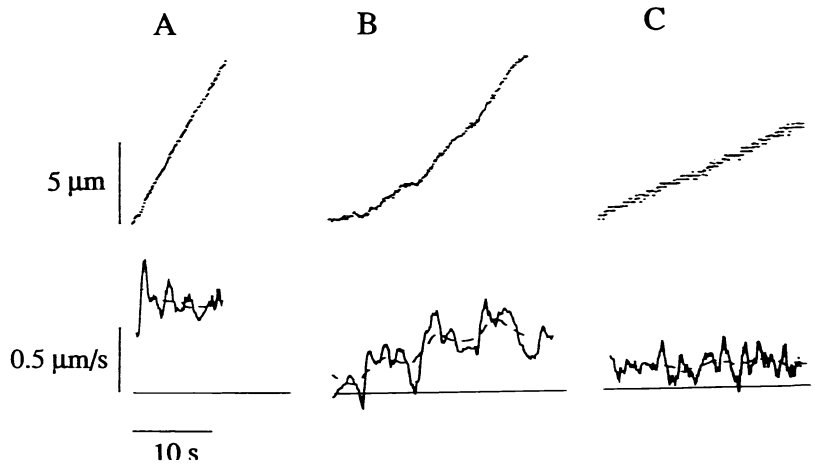

FIGURE 5 (*top*) Position versus time traces of microtubules moving through visc-mix at high (*A*), medium (*B*), and low (*C*) kinesin density. (*bottom*) Speed versus time traces at high (*A*), medium (*B*), and low (*C*) kinesin density constructed from the corresponding data in the upper panels. The speeds were calculated by linear regression fits to the data in a sliding rectangular window moved along the data shown in the upper panels. The solid line corresponds a 17 data point window, whereas the dashed line corresponds to a 65-point window.

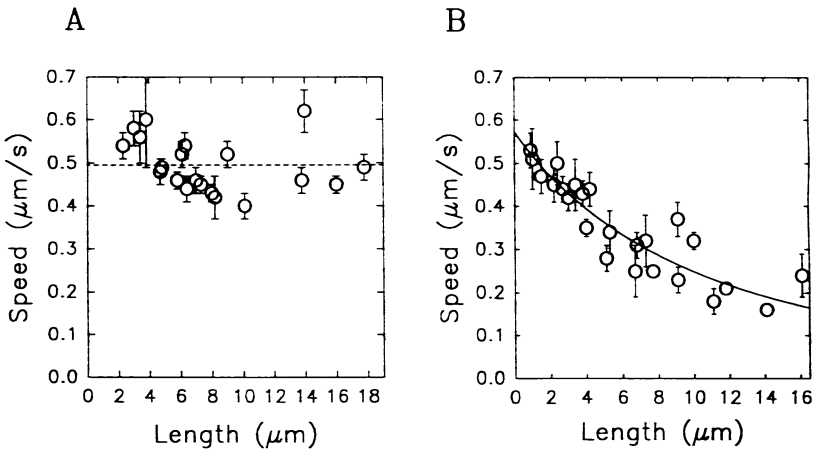

FIGURE 6 (*A*) At high kinesin density, when the viscosity was raised to approximately 100 times that of water (70% w/v visc-mix, η_0 = 59 mN·s·m^{-2}) the speed of translation remained independent of microtubule length. (*B*) At low kinesin density and the same viscosity as in *A*, the speed decreased with increasing microtubule length.

The decrease in microtubule speed is caused by viscous drag rather than a chemical effect

There are several reasons to believe that the slowing of the kinesin-driven movement is caused by the viscous drag on the microtubule rather than a chemical effect on the motor. Among the potential chemical effects are the following: it might take longer for ATP to diffuse to the motor's ATP-binding site; one of the physicochemical properties of the solution, such as its ionic strength or osmolality, might be different; or there could be some specific chemical effect of the solutes on the hydrolysis reaction. The most compelling argument against all of these potential effects is that an effect on the motor cannot explain why, at low kinesin densities, the longer microtubules were slowed down to a greater extent (Fig. 6 *B*).

We did several control experiments to rule out specific chemical effects of visc-mix on the motility. First, the slowing was not caused by insufficient ATP because a 10-fold increase in the Mg-ATP concentration had no effect on the speed of microtubule translation in 70% visc-mix; at high kinesin density, the average speed was 0.49 ± 0.02 μm·s^{-1} in 1 mM Mg-ATP, and 0.45 ± 0.02 μm·s^{-1} in 10 mM Mg-ATP. This is consistent with biochemical studies that show that the binding of ATP is not diffusion-limited: the second-order on-rate constant of 2.5 μM^{-1}·s^{-1} (Hackney et al., 1989) is perhaps 100-fold smaller than the diffusion limit and likely arises from a slow isomerization step that follows the initial diffusion-limited encounter (Hackney et al., 1989). Thus, even a 100-fold decrease in the mobility of ATP is not expected to have a dramatic effect on the on-rate.

Second, the decreased speed of microtubule translation through visc-mix was not caused by the increased osmolality of visc-mix compared with the standard buffer solution: microtubule translation was not significantly changed when the osmolality of the standard assay buffer (188 mOsm) was raised as high as 650 mOsm, well above the osmolality of even 90% visc-mix (426 ± 8 mOsm), by the addition of dextrose.

Third, it is also unlikely that the ionic strength of visc-mix caused microtubules to slow. The conductivity of visc-mix diluted to 10% with distilled water was 1275 ± 1 μS/cm, little different from the conductivity of a 10% solution of standard buffer (1286 ± 1 μS/cm). This implies that the concentration of free salts in visc-mix is at most a few percent different from that in standard buffer. The associated change in ionic strength is not likely to affect the speed because decreasing or increasing the ionic strength of standard buffer by 20% by dilution with water or by addition of KCl caused

little change in speed (speed = 0.71 ± .01 $\mu m \cdot s^{-1}$ in standard buffer, 0.73 ± 0.02 $\mu m \cdot s^{-1}$ in 80% standard buffer, 20% water, 0.66 ± 0.01 in standard buffer plus 50 mM KCl).

Finally, we performed a direct experiment to test whether the slowing at high kinesin density was caused by the viscosity of visc-mix or to the chemical composition of visc-mix. The speed of movement of microtubules in the high density assay in 93% visc-mix (η_0 = 209 $mN \cdot s \cdot m^{-2}$) was 0.21 $\mu m \cdot s^{-1}$, only about 20% of that in standard buffer solution (Fig. 7). The viscosity was then decreased by enzymatically cleaving the dextran in the mixture with dextranase. This decreased the viscosity of visc-mix by more than 10-fold (η_0 = 15.2 $mN \cdot s \cdot m^{-2}$) in a way that minimized other changes in the chemical environment. The speed of microtubule translation through dextranase-treated visc-mix increased more than fourfold to 0.87 $\mu m \cdot s^{-1}$, close to the translation speed in the absence of visc-mix (Fig. 7). This suggests that even the visc-mix-induced slowing at high kinesin density is caused by an effect of the increased viscosity on the motor rather than a chemical effect of the solutes on the motor.

The force-velocity curve

Because kinesin always generates a force parallel to the microtubule's protofilament axis (Hunt and Howard, 1993a; Ray et al., 1993), which very nearly parallels the long axis of the microtubule, the drag force can be calculated from

$$\langle F_{drag} \rangle = \Gamma \langle v \rangle = C_\parallel \eta L \langle v \rangle, \quad (2)$$

where η is the viscosity, L is the microtubule's length, $\langle v \rangle$ is the average speed of translation, and $C_\parallel$ is the dimensionless drag coefficient (drag per unit length per unit viscosity) for motion parallel to the microtubule's axis. Because $C_\parallel$ depends on the unknown height of the microtubule above the kinesin-coated surface (Appendix A), we measured this drag coefficient to be 7.0 ± 0.7 from analysis of the rotational diffusion in visc-mix of microtubules tethered to the surface by a single kinesin molecules (see Materials and Methods). This served as an almost direct calibration of the viscous force. The viscosity of the visc-mix solution was measured using a cone-and-plate viscometer and, because the fluid was non-Newtonian (Fig. 2), the drag force was computed numerically (Appendix B).

For each microtubule in Fig. 6 *B*, the drag force was computed from its length and speed. The resulting "force-velocity" curve, in which the speed of a microtubule was plotted against the drag force acting on it, shows that the greater the drag force on the microtubule, the slower the speed (Fig. 8). Within the uncertainty of the data, the speed depended linearly on the viscous force. Kinesin was able to translate microtubules against viscous loads greater than 3.5 pN and, by linear extrapolation, we estimate that the viscous drag force approaches 4.2 ± 0.5 pN as the speed of movement decreases to zero.

Limiting dilution

One of the goals of this study was to measure the force generated by a single kinesin molecule. The kinesin density used for the force-velocity curve was low (1–100 μm^{-2}), and we tentatively conclude that the forces correspond to single motors. Indeed, had these low densities been used in the low viscosity assay, we would have seen the pivoting behavior characteristic of movement by single kinesin molecules (Howard et al., 1989; Hunt and Howard, 1993a). However, for the longer microtubules at high viscosity, the diffusive pivoting of a microtubule about the point where the single kinesin motor is located is too slow to be detected reliably.

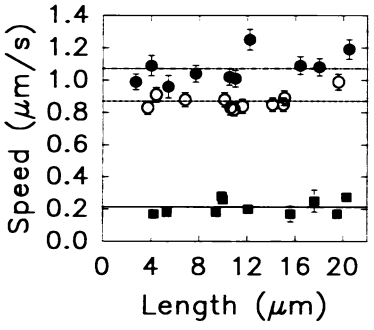

FIGURE 7 The speed of microtubule translation through visc-mix increased after the viscosity of visc-mix was lowered by dextranase. Closed squares are the translation speed in 93% visc-mix (η_0 = 209 $mN \cdot s \cdot m^{-2}$), open circles are in 93% dextranase-treated visc-mix (η_0 = 15.2 $mN \cdot s \cdot m^{-2}$), and closed circles are in standard buffer (0% visc-mix, η_0 = 0.8 $mN \cdot s \cdot m^{-2}$).

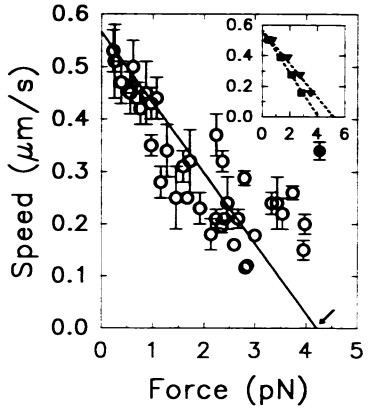

FIGURE 8 The relation between the viscous force and the speed of kinesin-driven microtubule translation at low kinesin density. The line is an unweighted least-squares fit to the data, and the extrapolated maximum single motor force is indicated by the arrow. The uncertainty in the linear extrapolation was 0.2 pN, which when combined with the uncertainty of 0.4 arising from the error in $C_\parallel$ gives a total error of 0.5. The intercept with the ordinate was fixed to be the same as in Fig. 6 *B*. The data point indicated by the closed circle was assumed to represent movement driven by more than one kinesin molecule and was not used in the least-squares fit. The surface density of kinesin was at or below 100/μm^2 in the assays used to construct this figure. Inset figure shows the force-velocity relation recalculated according to different speed profiles: the triangles correspond to a constant speed (Fig. 10 *A*), whereas the squares correspond to the exponential profile of Fig. 10 *C* (see Discussion).

Because this most important criterion for single-motor motility was not available in the high viscosity assay, we obtained additional, independent evidence that the motion was caused by single kinesin molecules.

The first strong indication that the motion at low kinesin density and high viscosity was caused by single molecules came from the smoothness of the motion at the lowest kinesin densities (Fig. 5 *C*). As the kinesin density was reduced from high to intermediate, the speed of microtubule movement became more variable as it became slower (Fig. 5, *A* and *B*). This variability in speed at intermediate kinesin densities is consistent with a variability in the number of motors moving the microtubule: if the average number of motors moving a microtubule were only two or three, then we would expect that as the microtubule moved across the surface the number of motors would vary, sometimes decreasing and sometimes increasing. If the drag force is significant compared with the single-motor force, we might then expect the speed to decrease and increase as the number of motors cooperating in the movement decreased and increased. On the other hand, if the motion were caused by a single motor, then we would expect a smooth, stereotyped motion. The increase in variability of the speed from high to intermediate kinesin density (Fig. 5 *B*), followed by the decrease in variability at the lowest kinesin densities (Fig. 5 *C*), is consistent with the motion being caused by a handful of motors and one motor, respectively. Unfortunately, our velocity resolution was not good enough to unequivocally detect quantized speeds at intermediate densities, although in all six experiments in which we analyzed the speed in greater detail we detected a significant increase in variability of speed at intermediate densities compared with high and low densities.

To obtain further evidence that at low kinesin density microtubules were indeed translated by single kinesin molecules, we estimated the force necessary to stop movement as a function of the kinesin density (Fig. 9). As the kinesin density was decreased below 1000 μm^{-2}, the force also decreased. But when the kinesin density was decreased below 100 μm^{-2}, no further decrease in force was apparent. This asymptotic behavior indicates that a minimum force level has been encountered; therefore, we interpret this force, approximately 4–5 pN, as the single-motor force.

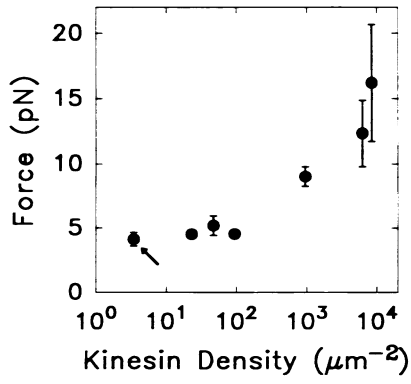

FIGURE 9 The extrapolated maximum force (determined as shown in Fig. 8) decreased to a minimum value of 4–5 pN as the kinesin density was decreased below 100/μm^2. The point indicated by the arrow was calculated using the data shown in Fig. 6 *B*.

DISCUSSION

The force exerted by a single kinesin molecule

The movement of microtubules across glass surfaces sparsely coated with kinesin was perturbed by raising the viscosity of the solutions. In high viscosity solutions, the longer microtubules moved more slowly than the shorter ones, indicating that the decrease in the speed of movement was caused by the viscous drag force acting on the microtubule, rather than by a chemical effect of the solution on the motor. The speed of movement of a microtubule depended linearly on the drag force acting on the motor (Fig. 8). At the lowest kinesin density, where dilution experiments indicated that the movement was caused by single kinesin molecules (Fig. 9), extrapolation of the linear relationship yielded a maximum time-averaged drag force of 4.2 ± 0.5 pN per motor (mean ± experimental SE). We believe that this force corresponds to the largest steady-state (or isotonic) force that a single kinesin molecule can exert against a viscous load.

One possible reservation is that because the kinesin molecules adsorbed to the surfaces with random orientations, this force might be an underestimate because of non-optimally oriented kinesin molecules. However, the extreme torsional flexibility of kinesin (Hunt and Howard, 1993a) makes it unlikely that the motor's force depends strongly on the motor's orientation. Nevertheless, it is still possible that the deviations of the points from the regression line in force-velocity data (Fig. 8) are caused by heterogeneity of kinesin molecules; if this is the case, the strongest motors might produce forces up to 6 pN. Another issue is that the majority of the microtubules used in these experiments had 14 protofilaments and are expected to rotate (Ray et al., 1993). But the rotation is so slow that the force required to overcome the rotational drag (Appendix A) is only about 4% of that required to overcome the translational drag; therefore, we have ignored the rotatory component.

A second, perhaps more serious concern is the uncertainty in the estimation of the viscous force acting on a microtubule. Because the diameters of the solute molecules (3.5, 6.4, and 16 nm) were not small in comparison with the diameter of the microtubules (~30 nm), we could not assume that the macroscopic viscosity of the solution, as measured with a cone-and-plate viscometer, was applicable for calculating the drag force acting on the microtubule. Therefore, we measured the "microscopic" viscosity by measuring the Brownian motion of microtubules in the visc-mix solution and found good agreement with the macroscopic viscosity (Table 1). In particular, we found no evidence that visc-mix displayed gel-like behavior. Another potential source of uncertainty in the drag force was the "wall effect" caused by the proximity of the microtubules to the kinesin-coated surface. To circumvent this problem, we directly measured the drag coefficient from the diffusion of microtubules tethered

at the same distance from the surface by kinesin molecules. This drag coefficient, which most closely approximated the drag coefficient experienced in the motility assay, was then used to calculate the drag force.

A final uncertainty in the estimation of the viscous force arises from the non-Newtonian behavior of the visc-mix fluid. Unlike a Newtonian fluid, for which the drag force depends linearly on the microtubule velocity (Eq. 2), the drag force in the non-Newtonian visc-mix depends nonlinearly on the velocity (Eq. B4). This introduces an added complication: the calculated drag force depends on the profile of the instantaneous velocity, and so the drag force depends on the particular model used to analyze the data. For example, if the microtubule speed varied during each hydrolysis cycle, sometimes being greater than the average speed and sometimes less, then the average drag force would be slightly smaller than if the motor had moved the microtubule at a steady speed. This model dependence is small, especially when the drag force is high, and we estimate that the maximum force is in the range 4.0–5.2 pN (Appendix D).

Comparison with other work

Several other laboratories have made force measurements on small numbers of motor proteins in vitro, although in no case has strong evidence been presented that the responses are caused by single molecules. Several devices have been used: force fibers (Ishijima et al., 1994), optical traps (Block et al., 1990; Finer et al., 1994; Kuo and Sheetz, 1993; Svoboda et al., 1993), and flexible filaments (Gittes et al., 1994) place elastic loads on the motor; the centrifugal microscope imposes an inertial load (Oiwa et al., 1990; Hall et al., 1993); and our technique creates a viscous load. Because the force exerted by a motor protein can depend on the nature of the load, it is interesting to compare our results with those obtained using different techniques.

Our single-motor force measurement lies within the range of forces reported to be exerted by kinesin against an optical trap; Svoboda et al. (1993) report a "nominal" $\langle F \rangle_{max} \geq 5$ pN, whereas Kuo and Sheetz report $\langle F \rangle_{max} = 1.95 \pm 0.4$ pN. Our result might be consistent with the former measurement. One possible reason why the Kuo and Sheetz force is lower than our force or the force of Svoboda et al. is that they used either GTP or a low concentration of ATP, whereas the other two studies used ATP at high concentration. Alternatively, the discrepancy might result from unbounded errors in the calibration of the optical tweezers: in both studies, the trap was used on motors very close (within a wavelength) of a high-refractive-index surface, but calibrated some distance from the surface. This leads to uncertainty of unknown magnitude (Howard, 1993).

Our results are not compatible with the value of 0.12 ± 0.03 pN that Hall et al. (1993) measured as the inertial force necessary to stall a single kinesin molecule in a centrifuge microscope. We have two reasons to believe that something other than the inertial force stopped the motors: first, in the absence of the inertial force the drag force is larger than 0.12 pN; and second, the stalling was independent of the direction of the inertial force. In any case, as pointed out by Hunt and Howard (1993a), the torsional flexibility of kinesin precludes using this centrifuge microscope assay to measure the single-motor force of a plus-end-directed motor like kinesin.

Our single-motor force is consistent with preliminary force measurements made in our laboratory using an assay in which kinesin molecules adsorbed to the surface exert forces against and buckle microtubules bound to the surface at their minus end (Gittes et al., 1994). The motor force can be calculated from the length of the segment of microtubule that buckles and the known flexural rigidity or bending stiffness of the microtubules (Gittes et al., 1993).

The time-averaged force exerted by kinesin against a viscous load (4–5 pN at ~30°C) is of the same order of magnitude as the time-averaged force exerted by myosin molecules in a skeletal muscle fiber (2.8 pN per myosin at 4°C, Lombardi et al., 1992; 3.2 pN per myosin at 0°C, Bagshaw, 1993). Transient forces exerted by myosin in vitro of ~5 pN (Ishijima et al., 1994) and 1–7 pN (Finer et al., 1994) have been recorded: if each myosin head is generating force for a large fraction of its cycle time (Ishijima et al., 1994), then myosin's time-averaged force is similar to that of kinesin; but if the fraction is small (Finer et al., 1994), then the time-averaged force is smaller than that of kinesin.

Comparison with some specific models for force generation

We now consider some detailed models that specify how the motor actually gets to its next binding site, a distance d away, and show how the particular features of a *viscous* load should affect them. These models predict the maximum force and velocity in terms of molecular parameters, and we ask whether these predictions are consistent with our measurements. We consider four specific models, two "ratchet" models in which directed motion arises from the rectification of diffusion of either the microtubule or the motor, and two "power stroke" models in which the motor is assumed to contain an elastic element that suddenly shortens and becomes strained. Only the ratchet model that relies on microtubule diffusion can be ruled out by our data. The other ratchet model (similar to the Huxley, 1957 model) and the power-stroke models cannot be excluded by the present results.

To discuss the force-velocity relation for a viscous load, we assume for simplicity that the solution is Newtonian. The consequences of the non-Newtonian nature of visc-mix are considered in Appendix D. First, we note that in our assay the only force loading the motor is the viscous force

$$F_{motor}(t) = F_{drag}(t) = \Gamma v(t); \quad (3)$$

there is no external elastic load on the motor in our assay, and we can ignore any inertial reaction forces because the Reynolds number is very low ($R = \rho L v/\eta \sim 10^{-5}$, for $\rho \sim 10^3$ kg·m^{-3}, $L \sim 10$ μm, $\eta \sim 1$ mN·s·m^{-2}, and average speeds $v \sim 1$ μm·s^{-1}).

Ratchet models

• **A filament-diffusion model.** This model assumes that it is by diffusion of the filament that the motor gets to the next binding site. This is the " ratchet diffusion" model first formulated for actin and myosin by Braxton (1988) and Braxton and Yount (1989): to get directed movement, one thinks of the motor molecule as an intelligent, or "cool" pawl (Feynman et al., 1964) that permits the filament (the ratchet) to move only in the preferred direction. Braxton postulated that the directed motion was caused by cooperative interactions between different motors moving the one filament. Subsequently, Vale and Oosawa (1990) postulated that the directed motion was caused by temperature differences between the motor and the filament: they called this the "thermal ratchet" model. As pointed out by Leibler and Huse (1993), this heat-engine idea of Vale and Oosawa (1990) cannot work because the diffusion of heat is so rapid over the dimensions of a protein that the postulated thermal gradients would dissipate within picoseconds, a timescale much faster than the microsecond to millisecond timescales of the transitions between the different chemical states of the motor. The filament-diffusion model is not well defined in molecular detail: for example, how ATP hydrolysis is coupled to the motion is not specified. Nevertheless, the model is appealing because it takes only a very short time for a filament to diffuse a distance equal to the size of a protein subunit: the time that it takes a moderately long microtubule (say 10 μm, Fig. 4) to diffuse 8 nm in a low viscosity medium is only 0.5 ms ($C_{\|}\eta L d^2/2kT$), which is very short compared with the cycle time (~10 ms, the inverse of the rate of ATP hydrolysis). Thus, in low viscosity solutions, the speed of the motor-driven motion is compatible with an underlying diffusive process (Braxton, 1988; Braxton and Yount, 1989). However, as the viscosity is increased the diffusional time will increase, and we expect the speed of movement to decrease. In this way, the model can be tested.

In Appendix C, we derive an expression for the speed as a function of drag force: the maximum force is $2kT/d$, where d is the step size. Substituting d = 8 nm (see Introduction) yields $\langle F\rangle_{max}$ = 1 pN, which is much smaller than the measured value (Fig. 8). Indeed, even if we use the infinite-shear viscosity of visc-mix to calculate the drag force, the data of Fig. 8 are compatible with $\langle F\rangle_{max}$ = 1.8 pN. Thus, if the step size is 8 nm, *we can rule out this " ratchet" model because it predicts that the speed in high viscosity solutions would be significantly smaller than we observed.* This conclusion is supported by the observations that kinesin can buckle microtubules (Gittes et al., 1993, 1994) that are clamped and, therefore, unable to undergo such diffusive fluctuations, and by the finding of Svoboda et al. (1993) that the average time that kinesin spends detached from the filament is <72 μs. This time is too short for a 10-μm-long microtubule to diffuse through 8 nm, and even too short to diffuse through 4 nm.

• **A motor-diffusion model.** Rather than assuming that the binding site on the microtubule diffuses to the motor, in this model we assume that the motor diffuses to the next binding site. Specifically, we assume that the motor contains an elastic element that undergoes thermal fluctuations: when the spring has become extended through a distance d, the motor binds to the next site on the microtubule whereupon the microtubule starts moving through the fluid to relieve the strain. In this case, the motor is the ratchet and the microtubule (presumably in combination with the motor) is the pawl. This idea originates from Huxley (1957) and was reconsidered by Vale and Oosawa (1990) and Cordova et al. (1992) in terms of a "thermal ratchet" model. We tested the motor-diffusion model by raising the viscosity and, therefore, presumably slowing down the underlying diffusive processes.

In Appendix C, we derive a theoretical force-velocity curve for this model. Our treatment differs significantly from the details of the Huxley (1957) paper: we compute the diffusional time required for thermal motions to stretch the spring within the motor through a distance d (this time is analogous to $1/f$ of the original Huxley, 1957 model), as well as the time after binding for the microtubule-motor complex to relax in the viscous solution to the unstrained position, whereupon it releases (analogous to $1/g$). These times place bounds on the motor speed. With a step size of 8 nm, a spring constant of 1 mN/m gives a maximum force of 4 pN, consistent with our force-velocity curve. The motor-diffusion time in 70% visc-mix is about 5–10 ms, consistent with the slight decrease in the speed of short microtubules in the low-kinesin-density assay (Fig. 6 *B*), and of all microtubules moved in the high-kinesin-density assay (Fig. 6 *A*, where we expect the number of motors is high enough to overcome the drag force on the microtubule). In 90% visc-mix, the diffusional time is expected to be about 30 ms: this is consistent with the slow movement of the microtubules shown in Fig. 7 in the high-kinesin-density assay. We predict that in low viscosity solutions the diffusional time would only be about 0.1 ms. Thus, *the motor-diffusion model is consistent not only with data obtained at low kinesin density and high viscosity, but it also explains simply the viscosity dependence seen in the high-kinesin-density assays.* The important point is that even in high viscosity solutions, thermal fluctuations of the motor are sufficiently rapid for the motor to pick up the required strain in a time consistent ith the measured speeds. An earlier attempt by Eisenberg and Hill (1978) to rule out the Huxley (1957) model made the argument that the predicted motions were too slow; however, these authors used an unrealistic value for the thermodynamic efficiency of muscle (83%), and if a more well accepted value of 50% is used, their argument breaks down.

Power-stroke models

Our data are also consistent with power-stroke models. These models assume that the motor contains an elastic element (of stiffness κ) which, while attached to the microtubule, suddenly shortens through a distance δ (not necessarily equal to

the step size d) and becomes strained. Directed motion results when this strain is relieved as the motor relaxes. The primary difference between the power-stroke models and the motor-diffusion model is that strain is developed after binding in the former models rather than before binding as in the latter model. We consider two different examples of power-stroke models and show that both predict linear force-velocity curves with maximum forces consistent with our data; although neither explain why the maximum speed in the high-kinesin-density assay is decreased at high viscosity.

- **Leibler and Huse model.** Our results are consistent with a model solved by Leibler and Huse (1991, 1993). A crucial feature of this model is that the time spent in the force-generating, "strongly-bound" state does not increase with increasing load: the decreased speed at high load is not caused by a slowing of the hydrolysis cycle but, instead, is caused by a decrease in the distance moved while the motor is in its force-generating state. The model predicts (via their Eq. A32) a linear velocity-drag force relation with $\langle F\rangle_{max} = \kappa\delta/t_c k_{23}$ and $\langle v\rangle_{max} = \delta/t_c$. If k_{23}, the rate of leaving the strongly bound state, is rate-limiting for kinesin, as Leibler and Huse argue, then $t_c \approx 1/k_{23}$ and values for $\langle F\rangle_{max}$ and $\langle v\rangle_{max}$ consistent with our data are obtained with $\kappa = 0.5$ mN·m^{-1}, $\delta = 8$ nm, and $t_c = 14$ ms (this is not a unique solution because δ need not equal d). Even though the Leibler and Huse model makes the unrealistic assumption that there is a continuum of binding sites along the surface of the microtubule, it seems reasonable that the model could be extended to incorporate discrete binding sites: a spring constant of 0.5 mN/m means that only 1 kT of thermal energy is required to stretch the motor through 4 nm, the minimum distance to the nearest binding site (in one direction or the other) if the step size is 8 nm.
- **Escapement model.** Our results are also consistent with a model in which the time spent in the force-generating state depends on load. Specifically, we assume that the motor must move the microtubule through a distance equal to the step size (d) before leaving the force-generating state: completion of the biochemical reaction requires completion of the mechanical motion, analogous to the escapement mechanism of a clock (Huxley, 1981). This gives rise to the so-called Fenn effect (Bagshaw, 1993): the smaller the load, the greater the speed, and the greater the hydrolysis rate. This model is also solved in Appendix C: our measured maximum force of 4 pN is consistent with the model with $\kappa = 1$ mN·m^{-1}, $d = 8$ nm, and $\delta = 10$ nm (again these are not unique solutions because δ could be larger and κ smaller).

Efficiency of the motor

The work done per power stroke is on the order of $\langle F\rangle_{max} d$ (Appendix C), or 32×10^{-21} J for the escapement model. Given that the free energy associated with ATP hydrolysis under cellular conditions is about 80×10^{-21} J, our results indicate that the efficiency of the kinesin motor is about 40%, assuming that only one molecule of ATP is required for each step. The efficiency for the Leibler and Huse model is less than that of the escapement model.

Functional implications

The ability of kinesin to generate high force, perhaps even higher than that produced by myosin in muscle, is likely to be an adaptation for the intracellular transport of vesicles. The cytoplasm is so crowded by protein filaments that the mobility of organelles is greatly impeded. Using fluorescent tracer molecules of various sizes, Luby-Phelps et al. (1986) have estimated that the pores between the structural barriers in the cytoplasm are about 50 nm wide. Therefore, to drag larger-diameter vesicles through this matrix, it is necessary that kinesin generate sufficient force to push these structural barriers out of the way. Because organelles are moved by a relatively small number of motors (Miller and Lasek, 1985), it makes sense that each motor can generate a large force.

We especially thank T. Duke, D. Huse, and S. Leibler for their criticism of an earlier version of this manuscript. We also thank D. Coy, A. J. Hudspeth, and B. Mickey for their comments on the manuscript.

J. Howard was supported by National Institutes of Health (AR40593), the Alfred P. Sloan Foundation, and was a Pew Scholar in the Biomedical Sciences. F. Gittes was supported by a Mathematical Biology fellowship from the National Science Foundation (BIR 9256532).

APPENDIX A. DRAG FORCES ON A CYLINDER (NEWTONIAN CASE)

Cylinder near a wall

Here we collect some exact drag coefficients of relevance to in vitro motility assays. Although these expressions are simple, they do not seem be generally known in the biophysical literature; approximations to them (e.g., Brennen and Winet, 1977) have been in wide use.

In a motility assay, a microtubule can be modeled as a long cylinder (length L) whose axis is parallel to a wall and at a height h above it. The fluid motion can be treated as creeping flow (i.e., vanishing Reynolds number). Because the cylinder is very close to the wall compared with its length ($L/h \gg 1$), the drag per unit length is essentially the same as if the cylinder had infinite length. We pause to elaborate on this assertion.

For the motion of an infinite cylinder, the viscous drag arises almost entirely from shear dissipation taking place in the immediate vicinity of the cylinder; primarily between the cylinder and the wall (see Fig. 10). The viscous dissipation per volume falls off quickly, as the inverse fourth power, far from the cylinder-wall gap. In our case, this gap is about 10 nm (Hunt and Howard, 1993a). The localized dissipation implies that the total drag on a microtubule thousands of nanometers long, close to a wall, is essentially the same per unit length as if the length were infinite. Near the ends (tens of nanometers away), the drag per length might be less, but the length itself is unknown to this accuracy.

We risk belaboring this point because the situation is quite different when no wall is present. In such a case, the velocity profile near the microtubule falls off only logarithmically, and the drag per length of an infinite cylinder is undefinable (see Section 2).

The drag coefficients $c_{\parallel}$, $c_{\perp}$, and c_v denote the drag force per unit velocity per unit length of an infinite cylinder near a surface. They apply to creeping flow (i.e., vanishingly low Reynolds number), either steady or unsteady. (A2), (A3), and (A4) were originally derived by Jeffrey and Onishi (1981), and independently by F. Gittes. The cylinder radius is r, the height of the cylinder axis above the surface is h, and the dynamical viscosity of the fluid

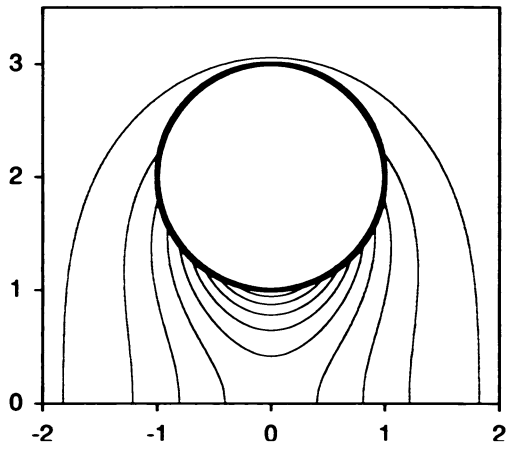

FIGURE 10 Lines of constant dissipation per unit volume caused by an infinite cylinder of unit radius ($r = 1$) moving parallel to its axis at a height $2r$ above a surface. The maximum dissipation is at the bottom of the cylinder. Relative to this maximum, contours are drawn at dissipation values of 0.9, 0.8, . . . , 0.1, and they show that dissipation is highly localized in the fluid.

is η. In the text, we use a capital $C_\parallel$, $C_\perp$, and C_v to denote the dimensionless values (drag per unit length per unit viscosity) obtained by dividing $c_\parallel$, $c_\perp$, and c_v by the viscosity η.

For motion parallel to the cylinder axis,

$$c_\parallel = 2\pi\eta/\cosh^{-1}(h/r) = 2\pi\eta/\ln[(h/r) + [(h/r)^2 - 1]^{1/2}]. \quad \text{(A1)}$$

This expression is obtained in Appendix B: it is valid at any Reynolds number if the flow is steady. It does not seem to appear explicitly in the literature.

For motion perpendicular to the cylinder axis and parallel to the wall,

$$c_\perp = 4\pi\eta/\cosh^{-1}(h/r) = 2c_\parallel. \quad \text{(A2)}$$

For vertical motion, meaning perpendicular to both the cylinder axis and the wall,

$$c_v = 1/[c_\perp^{-1} - c_a^{-1}], \quad \text{(A3)}$$

where $c_\perp$ is given by (A2) and c_a is the rotational drag coefficient, defined as follows: for rotation of the cylinder about its axis with angular velocity ω the drag torque per unit length is $c_a\omega r^2$, with coefficient

$$c_a = 4\pi\eta/[1 - (r/h)^2]^{1/2}. \quad \text{(A4)}$$

To complete the set of drag coefficients, we note that from $c_\parallel$ one can directly estimate the drag torque T of a long but finite cylinder ($L/h \gg 1$), rotating about a vertical axis located at a distance L_1 from one end and L_2 from the other, with $L_1 + L_2 = L$. For an angular velocity ω,

$$T \cong c_\perp\omega(L_1^3 + L_2^3)/3. \quad \text{(A5)}$$

Unlike the preceding results, however, this corresponds to no exact fluid solution.

Cylinder in an unbounded fluid

When no wall is present, we have pointed out that the drag per length of an infinite cylinder is undefinable (the "Stokes paradox"; see Happel and Brenner, 1965). As a consequence, a finite cylinder in solution must be treated as a finite three-dimensional object, with some overall drag coefficient (longitudinal, transverse or rotational). For creeping Newtonian flow, it is strictly speaking inappropriate to define a drag per unit length for a cylinder in an unbounded fluid.

We use a Γ to denote total drag coefficients for a particle, in contrast to the per-length drag coefficients given above. For a cylinder of length L in an unbounded fluid, with length-to-diameter ratio $p = L/2r$,

$$\Gamma_\parallel = \frac{2\pi\eta L}{\ln p + \gamma_\parallel}, \quad \text{(A6)}$$

$$\Gamma_\perp = \frac{4\pi\eta L}{\ln p + \gamma_\perp}, \quad \text{(A7)}$$

$$\Gamma_r = \frac{\frac{1}{3}\pi\eta L^3}{\ln p + \gamma_r}. \quad \text{(A8)}$$

$\Gamma_\parallel$ and $\Gamma_\perp$ are the total translational drag coefficients of the cylinder for motion along and perpendicular to the cylinder axis, respectively. For a rotation with angular velocity ω about an axis perpendicular to the cylinder axis, the drag torque is $\Gamma_r\omega$.

The end-correction terms $\gamma_\parallel$, $\gamma_\perp$, and γ_r are not constant but, in fact, depend on the axial ratio $p = L/2r$. Various approximations for these terms are available. We used formulae from Broersma (1981, their Table I; note $\sigma = \ln(2p)$, and our symbol γ is $\ln(2) - \gamma$ in his notation; see also his earlier calculations (Broersma, 1960a, b)). For $p = \infty$, these give limiting values $\gamma_\parallel = -0.114$, $\gamma_\perp = 0.886$, and $\gamma_r = -0.447$. A different calculation was carried out by Tirado and García de la Torre (1979; Table I, and 1980; Table II, where γ_r is denoted by $\delta_\perp$) whose numerical results differ from and might be more accurate than the formulae of Broersma. For $p = \infty$, they find similar limiting values: $\gamma_\parallel = -0.20$, $\gamma_\perp = 0.84$, and $\gamma_r = -0.662$. Other relevant references can be found in Tirado and García de la Torre (1979, 1980).

APPENDIX B. NON-NEWTONIAN DRAG FORCE

We turn specifically to the calculation of drag force on a microtubule moving parallel to its own axis near a surface. To find this force, one solves for the pattern of fluid flow assuming an infinite cylinder. Doing this for a Newtonian fluid, we will obtain the formula (A1) of Appendix A. However, the fluid used in our experiment is non-Newtonian; the viscosity as measured in a viscometer depends strongly upon shear rate in the low-shear regime. Therefore, we will generalize the calculation to a non-Newtonian fluid flow.

Fortunately, for longitudinal motion one has simple shear flow, i.e., one can write the velocity as $v(x, y)$, where the xy-plane is perpendicular to the cylinder. One can show (Astarita and Marrucci, 1974) that such flow can be described as a "generalized Newtonian fluid." As a consequence, if we write the stress tensor as a vector σ in the xy-plane, it is proportional to the gradient s of the velocity v,

$$\sigma = \eta s, \qquad s = \nabla v.$$

This is just as for a Newtonian fluid, except that the generalized viscosity η depends on the shear rate $s = |s|$,

$$\eta = \eta(s).$$

The shear-dependent $\eta(s)$ measured in a viscometer directly applies to the drag flow of the microtubule moving near the wall. The fluid equation to be solved for steady flow is $\nabla \cdot \sigma = 0$, that is,

$$\nabla \cdot (\eta(s)\nabla v) = 0, \qquad s = |\nabla v|. \quad \text{(B1)}$$

This equation is to be solved in the (x, y)-plane perpendicular to the cylinder, for the velocity $v(x, y)$ in the direction parallel to the cylinder. The boundary conditions are that $v = 0$ on the wall, $y = 0$, and $v = V$ on the cylinder, $x^2 + (y - h)^2 = r^2$.

We first note that in the Newtonian case, where η is independent of s, (B1) simply becomes Laplace's equation, $\nabla^2 v = 0$. The solution with correct boundary conditions is easily found by superposition of images,

$$v(x, y) = (V/2)(v_+ - v_-)/\cosh^{-1}(h/r), \quad \text{(B2)}$$

$$v_\pm = \ln[x^2 + (y \pm [h^2 - r^2]^{1/2})^2] \qquad \text{(Newtonian case)}.$$

Integrating the shear stress $\sigma = \eta\partial v/\partial y$ over the wall at $y = 0$, one obtains the drag coefficient $c_\parallel$ given by (A1) of Appendix A. The rate of dissipation of energy per volume shown in Fig. 1 *A* is given by $\eta[(\partial v/\partial x)^2 + (\partial v/\partial y)^2]$.

Turning to the non-Newtonian solution, we must solve equation (B1) for a shear-dependent $\eta(s)$. As discussed in the text (see Materials and Methods), the viscosity η rises to infinity at low shear, and can be fit either by a model with a small yield stress or by a constant plus an inverse power of s; both include the divergence at $s = 0$. However, the two solutions will only differ far from the cylinder where $\sigma = \sigma_y$; the yield-stress model will have v become zero at this point. Because the yield-stress boundary condition is awkward, we use the power-law form for our drag calculation:

$$\eta(s) = \eta_0(1 + (s_0/s)^{0.75}); \tag{B3}$$

typical values are $\eta_0 = 80$ mN·s·m^{-1} and $s_0 = 20$ s^{-1}. Although $\eta(s)$ becomes infinite at small s, the actual drag force per area $F = s\eta(s)$ does go to zero as the shear s goes to zero.

Equation (B1) is a nonlinear partial differential equation. It was solved numerically by conformally mapping the entire (x, y)-plane external to the wall and cylinder to a rectangle, using bipolar cylinder coordinates (Morse and Feshbach, 1953). The derivatives of v and η were approximated on a rectangular grid in these coordinates, and a relaxation procedure converged to the solution $v(x, y)$ with increasing grid density. The result, for $m = 0.75$ in (B3), and with a cylinder axis-height-to-radius ratio of $h/r = 1.43$, was a drag force on the cylinder per unit length of

$$F(V) = c_0 V[1 + (V_0/V)^{0.75}], \tag{B4}$$

where

$$c_0 = 2\pi\eta_0 V/\cosh^{-1}(h/r),$$

$$V_0 = s_0 r\, A(V/s_0 r).$$

The dimensionless function $A(x)$ is a weak function of x, as seen from its calculated values in Table 2. For $V \gg s_0 r$, the first term in (B4) dominates, giving a Newtonian drag using c_0, with the high-shear-rate viscosity η_0, as in (A1) of Appendix A. For lower velocities, the power-law term in (B4) cannot be neglected.

APPENDIX C. MODELS FOR FORCE GENERATION

Filament-diffusion model

To derive a force-velocity curve, we make the assumption that the motor releases the filament at one binding site, and when the microtubule diffuses so that the next binding site (a distance d away in the direction of translation) lines up with the motor, the motor rebinds and completes the hydrolysis cycle. To obtain directed movement, we assume that the motor somehow acts as a reflecting boundary (a pawl) to prevent filament movement in the wrong direction. This assumption maximizes the speed for this class of models. The solution for the mean time, t_D, to first capture is well known (Berg, 1983):

$$t_D = \frac{d^2}{2D} = \frac{\Gamma d^2}{2kT},$$

where the second equality includes the relation $D = kT/\Gamma$ (see Materials and Methods). If the total duration of the hydrolysis cycle (t_c) were simply equal to t_D, then the average speed of microtubule movement

$$\langle v\rangle = d/t_c$$

would diverge at low drag ($\Gamma \to 0$). This is not consistent with our data (Figs. 6 *B* and 8). Therefore, we further assume that the hydrolysis cycle includes a stationary phase, of duration t_0, during which no movement occurs and which is therefore independent of viscosity and Γ. Thus,

$$t_c = t_0 + t_D.$$

Combining the above equations yields

$$\frac{1}{\langle v\rangle} = \frac{t_c}{d} = \frac{t_0}{d} + \frac{\Gamma d}{2kT}.$$

In terms of the drag force $\langle F_{drag}\rangle = \Gamma\langle v\rangle$ (see Eq. 3), this becomes upon eliminating Γ

$$\frac{\langle F_{drag}\rangle}{\langle F\rangle_{max}} = 1 - \frac{\langle v\rangle}{\langle v\rangle_{max}},$$

where

$$\langle F\rangle_{max} = \frac{2kT}{d} \quad \text{and} \quad \langle v\rangle_{max} = \frac{d}{t_0}.$$

$\langle F\rangle_{max}$ is the extrapolation of the time-averaged force to zero speed ($\Gamma \to \infty$, $\langle v\rangle \to 0$), and $\langle v\rangle_{max}$ is the speed of translation at zero load ($\Gamma \to 0$).

A motor-diffusion model

The average time, t_K, for a spring of stiffness κ to become stretched a distance equal to the step size d as a result of thermal fluctuations is

$$t_K = \frac{\Gamma_K}{\kappa}\sqrt{\frac{2\pi kT}{\kappa d^2}}\exp\left(\frac{\kappa d^2}{2kT}\right)$$

(Kramers, 1940, considering a profile like that of his Fig. 2 but with an abrupt decrease to the right of point C) where Γ_K in our case is the damping coefficient of the kinesin head ($\Gamma_K \cong 6\pi\eta r \cong 6 \times 10^{-9}$ N·s·m^{-1} for $r \cong 5$ nm). After the motor binds with this strain, the microtubule will move; the average time, t_R, for the motor-microtubule complex to relax back to the unstrained state is approximately

$$t_R \cong \frac{\Gamma}{2\kappa}\left[\ln\left(\frac{2\kappa d^2}{kT}\right) + \gamma\right]$$

(for $d > (kT/\kappa)^{1/2}$, derived from Wang and Uhlenbeck, 1945; Eq. 82) where $\gamma \cong 0.577$ is Euler's constant. As above, we divide the cycle time into the various components:

$$t_c = t_0 + t_R + t_K,$$

where again t_0 corresponds to a stationary phase as discussed above. When analyzing the speeds of microtubules of various lengths, we again obtain a linear force-velocity curve with

$$\langle v\rangle_{max} = \frac{d}{t_0 + t_K}, \quad \text{and} \quad \langle F\rangle_{max} = \frac{2\kappa d}{\ln(2\kappa d^2/kT) + \gamma}.$$

Note that because t_K is proportional to viscosity, $\langle v\rangle_{max}$ decreases with viscosity independent of microtubule length.

Escapement model

To solve this model, note that the moving phase of the cycle is completed only when the microtubule moves through the distance d to the next binding site; its duration, therefore, is

$$t_m = (\Gamma/\kappa)\ln(\delta/(\delta - d)), \qquad (\delta > d).$$

TABLE 2 Calculated values of $A = V_0/s_0 r$ vs. $x = V/s_0 r$, for $h/r = 1.43$

x	$A(x)$
0	1.29
0.01	1.32
0.1	1.41
1	1.63
10	2.03
100	2.73

If there exists a stationary phase of duration t_0 then we can write

$$t_c = t_0 + t_m.$$

Once again, we derive a linear force-velocity curve, where the maximum force is now

$$\langle F \rangle_{max} = \frac{\kappa d}{\ln[\delta/(\delta - d)]}.$$

If $\delta \gg d$, then the force and the velocity are constant during the moving part of the cycle, and the maximum force is $\kappa\delta$.

For the escapement model, the work done during the moving part of the cycle is

$$W = \kappa d(\delta - d) = \langle F \rangle_{max} d \cdot B(d/\delta),$$

where $B(d/\delta)$ is a dimensionless function; $B \geq 1$, $B(0) = 1$, $B'(0) = 0$, and $B \cong 1$ unless d/δ approaches one. For example, if $d = 8$ nm and $\delta = 10$ nm, then $B = 1.21$. For a maximum force of 4.2 pN, and a step size of 8 nm, we obtain a mechanical work $\geq 34 \times 10^{-21}$ J, corresponding to about $8kT$. The free energy available from ATP hydrolysis is $\sim 84 \times 10^{-21}$ J (calculated $\Delta G = \Delta G^\circ + RT \ln([ADP][P_i]/[ATP])$ from where R is the universal gas constant, and other values were obtained from Daniels and Alberty (1975) and Bagshaw (1993) for pH = 7.1, pMg = 3.3, $T = 37°C$, [ADP] = 0.02 mM, $[P_i]$ = 2 mM, and [ATP] = 4 mM).

APPENDIX D. ERRORS ARISING FROM THE NON-NEWTONIAN BEHAVIOR OF VISC-MIX

As mentioned earlier, the non-Newtonian behavior of visc-mix causes the time-averaged drag force to depend on the profile of the instantaneous speed during the cycle time. Thus, the force-velocity curve deduced from our experiments is model-dependent. The force-velocity curve shown in Fig. 8 was derived assuming that the microtubule moves at constant velocity during the moving phase of the cycle (t_m), and is stationary during t_0 (Fig. 11 *B*). Had we assumed instead that the microtubule moved at a constant speed throughout the cycle (Fig. 11 *A*), the right-hand curve in Fig. 8 (*inset*) would be obtained; the force-velocity curve is still linear, and the maximum force would be slightly higher at 5.2 pN. On the other hand, had we assumed a power-stroke model with $d = 8$ nm and $\delta = 8.6$ nm, in which the speed varied substantially during the cycle (Fig. 11 *C*), the left-hand curve in Fig. 8 inset would be obtained; the force-velocity curve is still linear and the maximum force would be slightly lower at 4.1 pN. This force is a lower bound because smaller values for δ would cause the work to exceed the free energy of hydrolysis. The average force is also relatively insensitive to the step size d; $\langle F \rangle_{max} = 4.3$ pN for $d = 4$ nm and $\delta = 5$ nm, and $\langle F \rangle_{max} = 4.0$ pN for $d = 16$ nm and $\delta = 17$ nm. These results show that the time-averaged force necessary to propel a microtubule at an observed average speed is relatively insensitive to the exact relation between force and time during a cross bridge cycle. Our estimate for the maximum single-motor force lies between 4.0 and 5.2 pN.

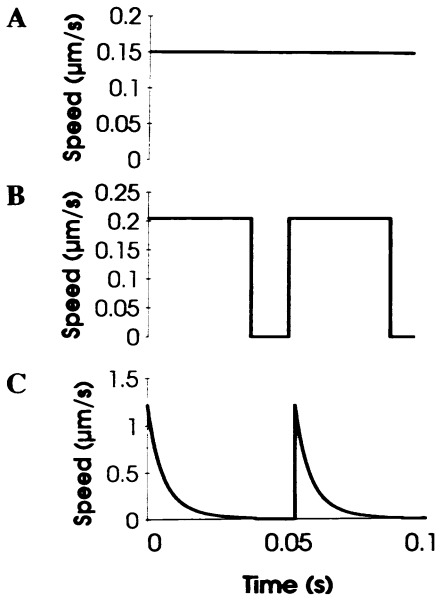

FIGURE 11 Three different speed profiles used to calculate the drag forces shown in Fig. 8. (*A*) The speed is constant throughout the hydrolysis cycle. (*B*) The speed is constant during the moving phase and zero during a stationary phase. (*C*) The speed relaxes during the moving phase as would be expected for a power-stroke model in which movement relieves the tension in an elastic element.

REFERENCES

Allen, R. D., D. G. Weiss, J. H. Hayden, D. T. Brown, H. Fujiwake, H., and M. Simpson. 1985. Gliding movement of and bidirectional movement along single native microtubules from squid axoplasm: evidence for an active role of microtubules in cytoplasmic transport *J. Cell Biol.* 100: 1736–1752.

Amos, L. A., and A. Klug. 1974. Arrangement of subunits in flagellar microtubules *J. Cell. Sci.* 14:523–549.

Astarita, G., and G. Marrucci. 1974. Principles of Non-Newtonian Fluid Mechanics. McGraw-Hill, London.

Bagshaw, C. R. 1993. Muscle Contraction. 2nd Ed. Chapman & Hall, New York.

Beese, L., G. Stubbs, and C. Cohen. 1987. Microtubule structure at 18 angstrom resolution *J. Mol. Biol.* 194:257–264.

Berg, H. 1983. Random Walks in Biology. Princeton University Press, Princeton, NJ.

Block, S. M., L. S. B. Goldstein, and B. J. Schnapp. 1990. Bead movement by single kinesin molecules studied with optical tweezers. *Nature.* 348: 348–352.

Brady, S. T. 1985. A novel brain ATPase with properties expected for the fast axonal transport motor. *Nature.* 317:73–75.

Braxton, S. M. 1988. Synthesis and Use of a Novel Class of ATP Carbamates and a Ratchet Diffusion Model for Directed Motion in Muscle. Ph. D. Thesis. Washington State University, Pullman, WA.

Braxton, S., and R. G. Yount. 1989. A ratchet diffusion model for directed motion in muscle. *Biophys J.* 55:12*a* (Abstr.)

Brennen, C., and H. Winet. 1977. Fluid mechanics of propulsion by cilia and flagella. *Annu. Rev. Fluid Mech.* 9:339–398.

Broersma, S. 1960a. Rotational diffusion constant of a cylindrical particle *J. Chem. Phys.* 32:1626–1631.

Broersma, S. 1960b. Viscous force constant for a closed cylinder *J. Chem. Phys.* 32:1632–1635.

Broersma, S. 1981. Viscous force and torque constants for a cylinder *J. Chem. Phys.* 74:6989–6990.

Cordova, N. J., B. Ermentrout, and G. F. Oster. 1992. Dynamics of single-motor molecules: the thermal ratchet model. *Proc. Natl. Acad. Sci. USA.* 89:339–343.

Daniels, F., and R. A. Alberty. 1975. Physical Chemistry. John Wiley & Sons, New York.

Fenn, W. O. 1924. The relation between the work performed and the energy liberated in muscular contraction. *J. Physiol. (Lond.).* 184: 373–395.

Feynman, R. P. 1964. The Feynman Lectures on Physics. R. B. Leighton and Sands. Addison-Wesley, Reading, MA.

Finer, J. T., R. M. Simmons, and J. A. Spudich. 1994. Single myosin molecule mechanics: piconewton forces and nanometer steps. *Nature.* 368: 113–119.

Gilbert, S. P., and K. A. Johnson. 1993. Expression, purification, and characterization of the Drosophila kinesin motor domain produced in *Escherichia coli*. *Biochemistry.* 32:4677–4684.

Gittes, F., B. Mickey, J. Nettleton, and J. Howard. 1993. Flexural rigidity of microtubules and actin filaments measured from thermal fluctuations in shape. *J. Cell Biol.* 120:923–934.

Gittes, F., E. Meyhöfer, S. Baek, and J. Howard. 1994. A simple piconewton-scale in vitro force assay for kinesin. *Biophys. J.* 66:312*a* (Abstr.)

Hackney, D. D. 1988. Kinesin ATPase: rate-limiting ADP release. *Proc. Natl. Acad. Sci. USA.* 85:6314–6318.

Hackney, D. D., A. Malik, and K. W. Wright. 1989. Nucleotide-free kinesin hydrolyzes ATP with burst kinetics *J. Biol. Chem.* 264:15943–15948.

Hall, K., D. G. Cole, Y. Yeh, J. M. Scholey, and R. J. Baskin. 1993. Force-velocity relationships in kinesin-driven motility. *Nature.* 364:457–459.

Happel, J., and H. Brenner. 1965. Low Reynolds Number Hydrodynamics. Prentice-Hall, Englewood Cliffs, NJ.

Harrison, B. C., S. P. Marchese-Ragona, S. P. Gilbert, N. Cheng, A. C. Steven, and K. A. Johnson. 1993. Kinesin decoration of the microtubule surface: one kinesin head per tubulin heterodimer. *Nature.* 362:73–75.

Hill, A. V. 1938. The heat of shortening and the dynamic constants of muscle. *Proc. R. Soc. Lond. B Biol. Sci.* 126:136–195.

Hirokawa, N., K. K. Pfister, H. Yorifuji, M. C. Wagner, S. T. Brady, and G. S. Bloom. 1989. Submolecular domains of bovine brain kinesin identified by electron microscopy and monoclonal antibody decoration. *Cell.* 56:867–878.

Hou, L., F. Lanni, and K. Luby-Phelps. 1990. Tracer diffusion in F-actin and Ficoll mixtures. *Biophys. J.* 58:31–43.

Howard, J. 1993. Wrestling with kinesin. *Nature.* 364:390–391.

Howard, J., A. J. Hudspeth, and R. D. Vale. 1989. Movement of microtubules by single kinesin molecules. *Nature.* 342:154–158.

Howard, J., A. J. Hunt, and S. Baek. 1993. Assay of microtubule movement driven by single kinesin molecules. *Methods Cell Biol.* 39:137–147.

Howard, J., and A. A. Hyman. 1993. Preparation of marked microtubules for the assay of the polarity of microtubule-based motors by fluorescence microscopy. *Methods Cell Biol.* 39:105–113.

Hunt, A. J., and J. Howard. 1993a. Kinesin swivels to permit microtubule movement in any direction. *Proc. Natl. Acad. Sci. USA.* 90:11653–11657.

Hunt, A. J., and J. Howard. 1993b. The force exerted by a kinesin molecule against a viscous load *Biophys. J.* 64:263*a*. (Abstr.)

Huxley, A. F. 1957. Muscle structure and theories of contraction *Prog. Biophys. Biophys. Chem.* 7:255–318.

Huxley, A. F. 1974. Muscular contraction *J. Physiol.* 243:1–43.

Huxley, A. F., and R. M. Simmons. 1971. Proposed mechanism of force generation in striated muscle. *Nature.* 233:533–538.

Huxley, A. F., and R. M. Simmons. 1972. Mechanical transients and the origin of muscular force. *Cold Spring Harbor. Symp. Quant. Biol.* 37: 669–680.

Huxley, A. F. 1981. Reflections on Muscle. Princeton University Press, Princeton, NJ.

Huxley, H. E. 1969. The mechanism of muscular contraction. *Science.* 164: 1356–1366.

Huxley, H. E., and M. Kress. 1985. Crossbridge behavior during muscle contraction *J. Muscle Res. Cell Motil.* 6:153–161.

Hyman, A., D. Drechsel, D. Kellogg, S. Salser, K. Sawin, P. Steffen, L. Wordeman, and T. Mitchison. 1991. Preparation of modified tubulins. *Methods Enzymol.* 196:478–485.

Ishijima, A., Y. Harada, H. Kojima, T. Funatsu, H. Higuchi, and T. Yanagida. 1994. Single-molecule analysis of the actomyosin motor using nano-manipulation. *Biochem. Biophys. Res. Commun.* 199:1057–1063.

Israelachvili, J. N. 1986. Measurement of the viscosity of liquids in very thin films. *J. Colloid Interface Sci.* 110:263–271.

Jeffrey, D. J., and Y. Onishi. 1981. The slow motion of a cylinder next to a plane wall *Quant. J. Mech. Appl. Math.* 34:129–137.

Kramers, H. A. 1940. Brownian motion in a field of force and the diffusion model of chemical reactions. *Physica.* 7:284–304.

Kron, S. J., and J. A. Spudich. 1986. Fluorescent actin filaments move on myosin fixed to a glass surface. *Proc. Natl. Acad. Sci. USA.* 83: 6272–6276.

Kuo, S. C., and M. P. Sheetz. 1993. Force of single kinesin molecules measured with optical tweezers. *Science.* 260:232–234.

Kuznetsov, S. A., Y. A. Vaisberg, S. W. Rothwell, D. B. Murphy, and V. I. Gelfand. 1989. Isolation of a 45-kDa fragment from the kinesin heavy chain with enhanced ATPase and microtubule-binding activities. *J. Biol. Chem.* 264:589–595.

Leibler, S., and D. A. Huse. 1991. A physical model for motor proteins. *C. R. Acad. Sci. Paris.* 313:27–35.

Leibler, S., and D. Huse. 1993. Porters versus rowers: a unified stochastic model of motor proteins. *J. Cell Biol.* 121:1357–1368.

Luby-Phelps, K., D. L. Taylor, and R. Lanni. 1986. Probing the structure of the cytoplasm. *J. Cell Biol.* 102:2015–2022.

Lymn, R. W., and E. W. Taylor. 1971. Mechanism of adenosine triphosphate hydrolysis by actomyosin. *Biochemistry.* 10:A4617–A4624.

Miller, R. H., and R. J. Lasek. 1985. Cross-bridges mediate anterograde and retrograde vesicle transport along microtubules in squid axoplasm. *J. Cell Biol.* 101:2181–2193.

Morse, P. M., and H. Feshbach. 1953. Methods of Theoretical Physics. McGraw-Hill, New York.

Oiwa, K., K. Chaen, E. Kamitsubo, T. Shimmen, and H. Sugi. 1990. Steady-state force-velocity relation in the ATP-dependent sliding movement of myosin-coated beads on actin cables in vitro studied with a centrifuge microscope. *Proc. Natl. Acad. Sci. USA.* 87:7893–7897.

Pate, E., and R. Cooke. 1991. Simulation of stochastic processes in motile systems. *J. Muscle Res. Cell Motil.* 12:376–393.

Ray, S., E. Meyhöfer, R. A. Milligan, and J. Howard. 1993. Kinesin follows the microtubule's protofilament axis. *J. Cell Biol.* 121:1083–1093.

Rayment, I., W. R. Rypniewski, K. Schmidt-Bäse, R. Smith, D. R. Tomchick, G. Wesenberg, and H. M. Holden. 1993. Three-dimensional structure of myosin subfragment-1: a molecular motor. *Science.* 261: 50–58.

Romberg, L., and R. D. Vale. 1993. Chemomechanical cycle of kinesin differs from that of myosin. *Nature.* 361:168–170.

Scholey, J. M., J. Heuser, J. T. Yang, and L. S. B. Goldstein. 1989. Identification of globular mechanochemical heads of kinesin. *Nature.* 338: 355–357.

Sheetz, M. P., and J. A. Spudich. 1983. Movement of myosin-coated fluorescent beads on actin cables in vitro. *Science.* 303:31–35.

Sheetz, M. F., S. M. Block, and J. A. Spudich. 1986. Myosin movement *in vitro*: a quantitative assay using oriented actin cables from *Nitella*. *Methods Enzymol.* 134:531–544.

Skelland, A. H. P. 1967. Non-Newtonian Flow and Heat Transfer. John Wiley & Sons, New York.

Svoboda, K., C. F. Schmidt, B. J. Schnapp, and S. M. Block. 1993. Direct observation of kinesin stepping by optical trapping interferometry. *Nature.* 256:721–727.

Sweet, R. M., H. T. Wright, J. Janin, C. H. Chothia, and D. M. Blow. 1974. Crystal structure of the complex of porcine trypsin with soybean trypsin inhibitor (Kunitz) at 2.6-angstrom resolution. *Biochemistry.* 13: 4212–4228.

Tirado, M. M., and J. Garcia de la Torre. 1979. Translational friction coefficients of rigid, symmetric top macromolecules. Application to circular cylinders. *J. Chem. Phys.* 71:2581–2587.

Tirado, M. M., and J. Garcia de la Torre. 1980. Rotational dynamics of rigid, symmetric top macromolecules. Application to circular cylinders. *J. Chem. Phys.* 73:1986–1993.

Vale, R. D., T. S. Reese, and M. P. Sheetz. 1985a. Identification of a novel force-generating protein, kinesin, involved in microtubule-based motility. *Cell.* 42:39–50.

Vale, R. D., B. J. Schnapp, T. S. Reese, and M. P. Sheetz. 1985b. Organelle, bead, and microtubule translocations promoted by soluble factors from the squid giant axon. *Cell.* 40:559–569.

Vale, R. D., and F. Oosawa. 1990. Protein motors and Maxwell's demons: does mechanochemical transduction involve a thermal ratchet? *Adv. Biophys.* 26:97–134.

Van Hold, K. E. 1985. Physical Biochemistry. Prentice-Hall, Englewood Cliffs, NJ. 166–172.

Wang, M. C., and G. E. Uhlenbeck. 1945. On the theory of Brownian motion II. *Rev. Mod. Phys.* 17:323–342.

Warshaw, D. M., J. M. Desrosiers, S. S. Work, and K. M. Trybus. 1990. Smooth muscle myosin cross-bridge interactions modulate actin filament sliding velocity in vitro. *J. Cell Biol.* 111:453–463.